Measurement of strong coupling constant from transverse momentum

Alireza Sepehri, Tooraj Ghaffary, and Mohammad Ebrahim Zomorrodian

Abstract: Data from e^+e^- annihilation into hadrons at the center of mass energy of 60 GeV are used to study the distribution of momentum components with respect to the jet axis. At high energies, the gluon emission that leads to three jet structures represents a gross violation of the parton model without gluons and finds a most natural interpretation if gluon bremsstrahlung is included. The coupling constant, α_s, is measured by two different methods, first by employing the jet clustering algorithm introduced by the JADE group. Using this method, the strong coupling constant is found to be 0.123 ± 0.004. Next, from the event shape distributions, we extract the strong coupling constant, α_s, and test its evaluation with energy scale. The results are consistent with the running of α_s, expected from QCD predictions. Averaging over different observables, the value of α_s is determined to be 0.121 ± 0.007.

PACS No: 13.66.Bc

Résumé : Nous utilisons les données d'annihilation de e^+e^- en hadrons à une énergie dans le centre de masse de 60 GeV, afin d'étudier la distribution des composantes de la quantité de mouvement par rapport à l'axe du jet. À haute énergie, l'émission de gluons qui mène à une structure à trois jets représente une violation majeure du modèle des partons sans gluons et trouve une explication toute naturelle si nous incluons le bremsstrahlung des gluons. Finalement, nous mesurons la constante de couplage α_S, en utilisant l'algorithme de regroupement de jets introduit par le groupe JADE. Avec cette méthode, nous déterminons que α_S a la valeur $0\,123 \pm 0\,004$. Cette valeur est cohérente avec les résultats provenant d'autres expériences.

[Traduit par la Rédaction]

1. Introduction

The role of a gluon jet in three-jet events has been previously studied by many collaborations and in various colliding systems, e^+e^- annihilations [1–4], hadron–hadron collisions [5], and deep inelastic scattering [6]. Three-jet production cross-sections and related event shape distributions in e^+e^- annihilation processes are classic hadronic observables, which can be measured very accurately and provide an ideal proving ground for testing our understanding of strong interactions. The deviation from simple two-jet configurations is proportional to the strong coupling constant, α_s, so that by comparing the measured three-jet rate and related event shapes with the theoretical predictions, one can determine the strong coupling constant α_s.

Quantum chromodynamics (QCD) is generally accepted to be the correct theory to explain interaction between quarks and gluons [7, 8]. In this theory, the strong force is mediated by the exchange of massless vector gluons between quarks. The strong coupling constant, α_s, depends on momentum transfer between quarks and gluons. In other words, it is estimated to decrease with an increase in the energy scale of the process. So at high-Q^2 processes, calculations based on perturbative theory are valid [9, 10]. However in experimental situations, this theory is not usually applicable. Hence, phenomenological models must be used. For this purpose, data from e^+e^- annihilations provide us with one of the cleanest ways of probing our quantitative understanding of QCD, giving us an opportunity to measure the strong coupling between quarks and gluons.

In this paper we analyze the momentum distributions of final hadrons to investigate the evidence for gluon radiation, leading to three-jet structures. We separate two- and three-jet events by using the jet clustering algorithm introduced by the JADE group [11, 12], and we measure the strong coupling constant α_s, considering the Altarelli–Parisi–Weizsacker–Williams technique [13].

Finally, we will measure the coupling constant considering event shape observables using next-to-next leading order (NNLO) calculations. The reason for doing such measurements is that in ref. 14 the strong coupling constant α_s has been determined from the measured moments of particle momenta within jets using a next-to-leading logarithm patron shower model. One might anticipate a priori that this method would yield a less precise determination of α_s than the differential distribution of event shape, because the theory lacks resummation of large logarithms, and the moments include regions of phase space where hadronization effects are large [15]. Nevertheless, the comparison of α_s determined in this way with that obtained from the differential event shape distribution should provide an illuminating test of the adequacy of QCD in this area.

Received 17 June 2009. Accepted . Published on the NRC Research Press Web site at cjp.nrc.ca on .

A. Sepehri, T. Ghaffary,[1] and M.E. Zomorrodian.[2] Ferdowsi University of Mashhad, School of sciences, Departement of Physics 91775, Mashhad, Islamic Republic of Iran.

[1]Corresponding author (e-mail: tooraj58@yahoo.co.uk).
[2]Corresponding author (e-mail: zomorrod@ferdowsi.um.ac.ir).

Fig. 1. The average momentum, $\langle P \rangle$, $\langle P_{\parallel} \rangle$, $\langle P_T \rangle$, $\langle P_T^2 \rangle$ averaged over all events as a function of c.m. energy W [17]. The curves show the prediction of the QCD model for $e^+e^- \to q\bar{q}$: $q\bar{q}g$ (solid), and $e^+e^- \to q\bar{q}$ (dashed).

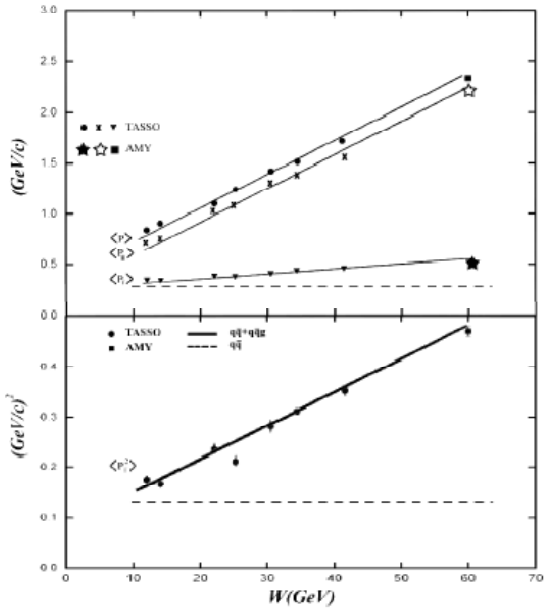

Fig. 2. The averaged momentum squared in and out of the event plane, $\langle P_{T\text{in}}^2 \rangle$ and $\langle P_{T\text{out}}^2 \rangle$ averaged over all events as a function of c.m. energy W [17]. The curves shows the prediction of QCD model for $e^+e^- \to q\bar{q}$, $q\bar{q}g$ (solid), and $e^+e^- \to q\bar{q}$ (dashed).

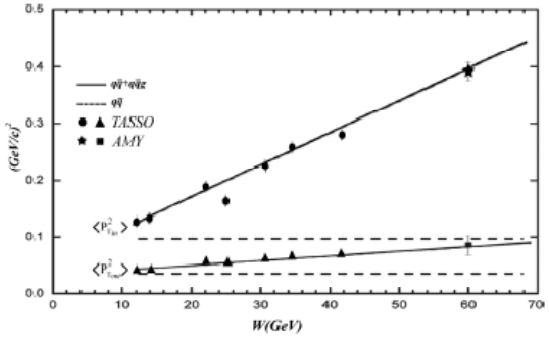

2. Experimental set up

The AMY detector consists of a tracking detector and shower counter inside a 3-T solenoid magnetic coil, which is surrounded by a steel flux return yoke followed by a muon detection system. The charged particle tracking detector consists of a 4-layer cylindrical array of drift tubes (inner tracking chamber, or ITC) and a 40-layer cylindrical drift chamber (CDC) with 25 axial layers of wires and 15 stereo layers. Charged particles are detected efficiently over the polar angle region $\cos\theta < 0.87$, with a momentum resolution of $\Delta_{p_T} = 0.7\% \times [p_T(\text{GeV}/c)]$. Radially outside of the CDC is a 15 radiation-length cylindrical electromagnetic calorimeter (barrel shower counter or SHC), which serves as a photon detector. The detector fully covers the angular region $\cos\theta < 0.73$. Selection of multihadron final states from e^+e^- annihilation was based on the charged particle momenta measured in the CDC and on the neutral-particle energy measured in SHC [16].

3. Jet definition and jet prescriptions

Since jets are characterized by a specific reference axis, it is natural to analyze the particles yield with respect to this axis. There are different methods to find the jet axis from the measured particles. One of the most efficient methods, which is widely used in particle physics, involves the sphericity axis. In this method we diagonalize the 3×3 momentum tensor,

$$T^{\alpha\beta} = \sum_{n=1}^{N} p_i^{\alpha} p_i^{\beta} \tag{1}$$

where P_i are the momentum vectors of all charged particle hadrons, and α and β are the coordinate indices. We now order the eigenvalues λ_k of $T^{\alpha\beta}$ so that $\lambda_3 \geq \lambda_2 \geq \lambda_1$ and call the corresponding eigenvectors $\hat{n}_3$, $\hat{n}_2$, $\hat{n}_1$. The sphericity axis is $\hat{n}_3$. Although in particular for events of low multiplicities, the reconstructed axis may be biased, it reproduces the direction of the original parton in general quite well and allows one to obtain a representative picture of the longitudinal and transverse properties of jets in electron–positron annihilation. We also define for the later application the average $\langle p_{\text{out}}^2 \rangle = \langle (\boldsymbol{p} \cdot \hat{n}_1)^2 \rangle$ and $\langle p_{\perp\text{in}}^2 \rangle = \langle (\boldsymbol{p} \cdot \hat{n}_2)^2 \rangle$ over all charged particles of an event as a measure of the momentum out of the plane and in the plane, respectively, in a direction perpendicular to the sphericity axis.

4. The average longitudinal and transverse components

Whereas the average longitudinal momentum increases roughly proportional to the center-of-mass (c.m.) energy, the transverse component increases only marginally. The measurements of the average transverse momentum from different experiments [17–20], including AMY detector are shown in Fig. 1. The average transverse momentum, $\langle P_T \rangle$, grows slowly, and the average longitudinal momentum, $\langle P_{\parallel} \rangle$, grows considerably for an increase of W from 14 to 60 GeV. This indicates that on average, the particles within a jet are more and more collimated with increasing energy. On the other hand, the growth of $\langle P_T^2 \rangle$ is much more prominent. It more than doubles in the same energy range, suggesting the change in P_T is due to particles with large momentum. Such a high P_T component arises naturally from a third jet and constitutes one of the prime indications of hard gluon emission.

To clarify further the situation, we analyze the transverse component in more detail by separating the momentum contribution *in* and *out* of the event plane, namely $\langle P_{T\text{in}}^2 \rangle$ and $\langle P_{T\text{out}}^2 \rangle$ defined previously. The measurements are displayed in Fig. 2 and show that the high transverse component is concentrated in the plane: $\langle P_{T\text{in}}^2 \rangle$ increases much more

Fig. 3. Two- and three-jet fractions for different Y_{cut}s.

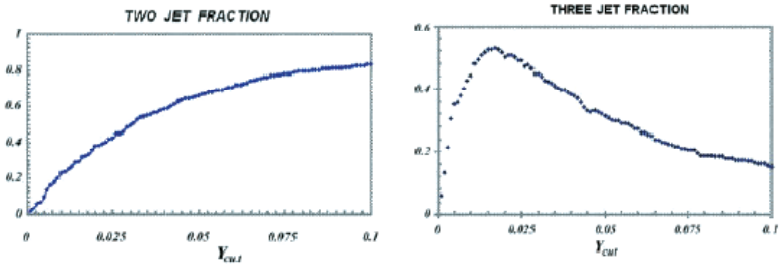

Fig. 4. The process $e^+e^- \rightarrow q\bar{q}g$ in the center of mass energy.

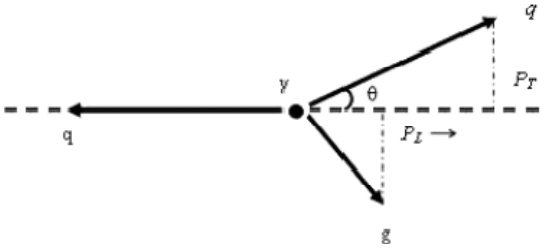

Fig. 5. Normalized cross-section for the square of the transverse component of momentum for $W = 60$ GeV.

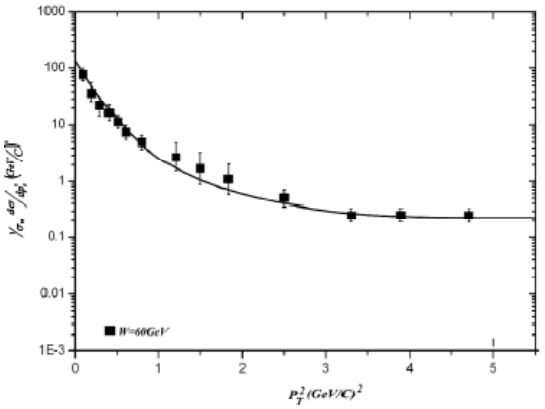

Table 1. α_s values for different Y_{cut}s according to the differential cross-section of three-jet events with respect to the P_T^2.

Y_{cut}	α_s
0.02	0.130±0.004
0.025	0.128±0.005
0.03	0.127±0.002
0.035	0.124±0.006
0.04	0.123±0.004
0.045	0.125±0.002
0.05	0.126±0.003

Fig. 6. Differential cross-section of three-jet events with respect to X_T^2. Data are compared with the prediction of QCD (solid line).

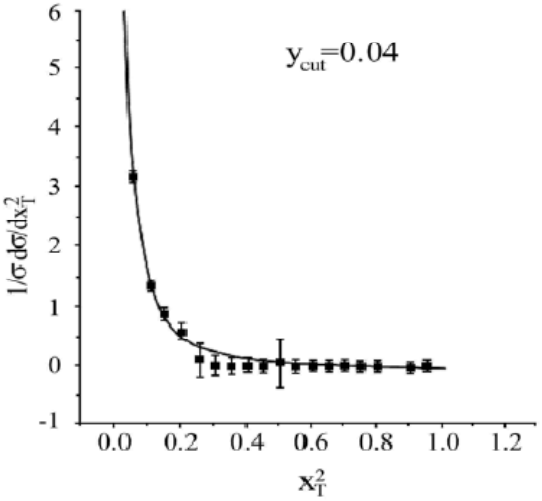

Table 2. α_s values for different Y_{cut}s according to the differential cross-section of three-jet events with respect to the X_T^2.

Y_{cut}	α_s
0.02	0.127±0.005
0.025	0.126±0.003
0.03	0.125±0.004
0.035	0.124±0.006
0.04	0.122±0.004
0.045	0.124±0.007
0.05	0.126±0.003

strongly than $<P_{Tout}^2>$. Also shown are the predictions from simulation studies with and without QCD bremsstrahlung [21]. Whereas the model without the hard gluon falls short of describing the rise of $<P_{Tout}^2>$, the results are very well reproduced by the models, including hard gluon bremsstrahlung.

It should be added that models without the emission of a hard gluon, but an increase of the transverse momentum of the hadrons do not reproduce the trend of the data. We con-

Fig. 7. The thrust distribution at LO (dotted), NLO (dashed), and NNLO (solid) compared with experimental data from AMY for Q = 60 GeV.

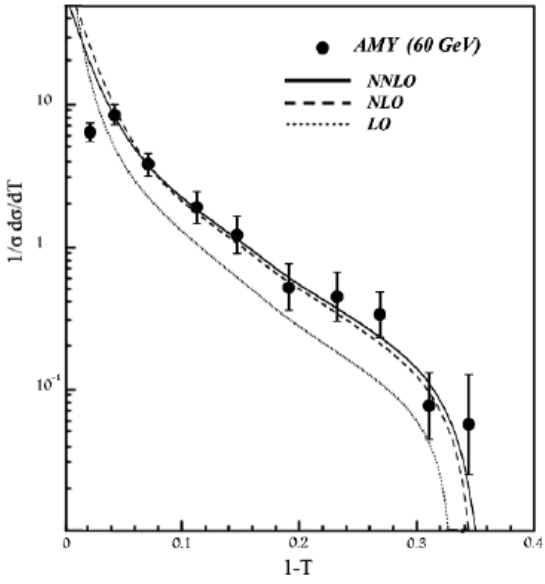

Fig. 8. Heavy jet mass distribution at LO (dotted), NLO (dashed), and NNLO (solid) compared with experimental data from AMY for Q = 60 GeV.

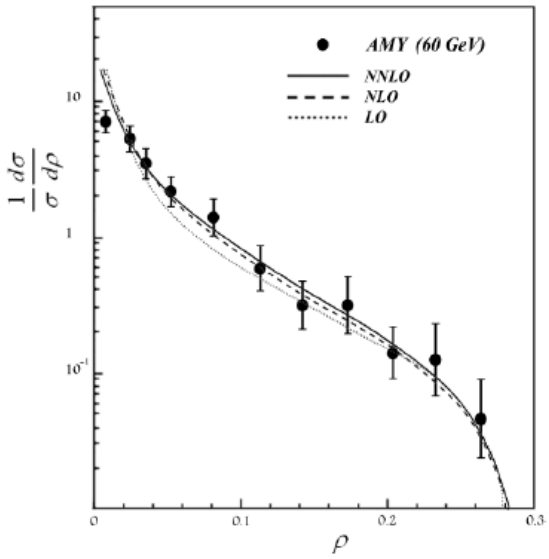

clude that there is a possibility of gluon radiation at high energies. This will lead us to three-jet events, namely two quark jets and one gluon jet.

Fig. 9. Total jet broadening distribution at LO (dotted), NLO (dashed), and NNLO (solid) compared with experimental data from AMY for Q = 60 GeV.

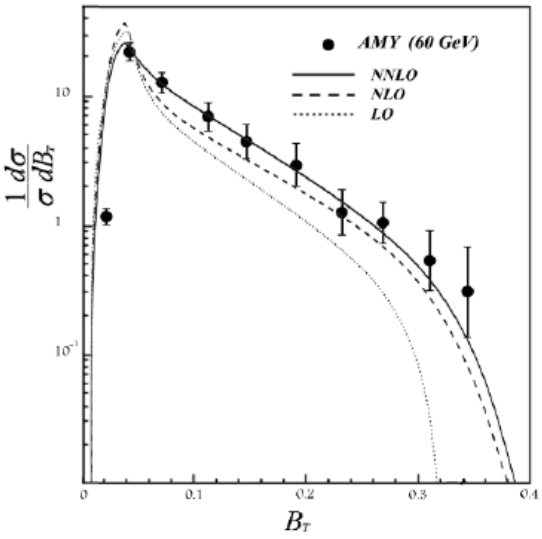

Fig. 10. Wide jet broadening distribution at LO (dotted), NLO (dashed), and NNLO (solid) compared with experimental data from AMY for Q = 60 GeV.

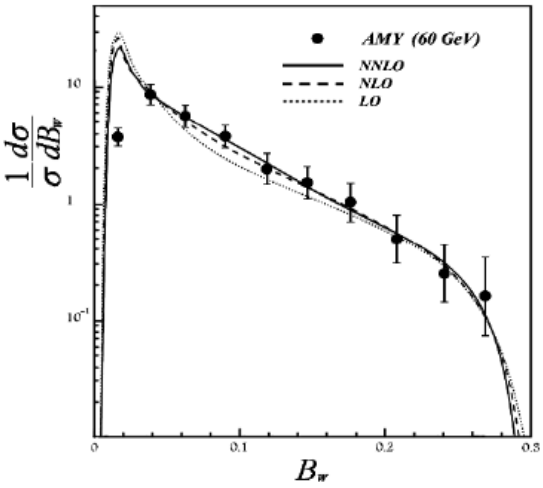

5. JADE algorithm

We separate two- and three-jet events by employing the jet clustering algorithm introduced by the JADE group [11]. In this algorithm, the scaled mass spread defined as $Y_{ij} = m_{ij}^2/E_{\text{vis}}^2$, where $m_{ij}^2 = 2E_iE_j(1-\cos\theta_{ij})$ is calculated for each pair of particles in the event. If the smallest of the Y_{ij} values is less than a parameter Y_{cut}, the corresponding pair of particles is combined into a cluster by summing the four momenta. This process is repeated, using all combina-

Fig. 11. *C*-parameter distribution at LO (dotted), NLO (dashed), and NNLO (solid) compared with experimental data from AMY for Q = 60 GeV.

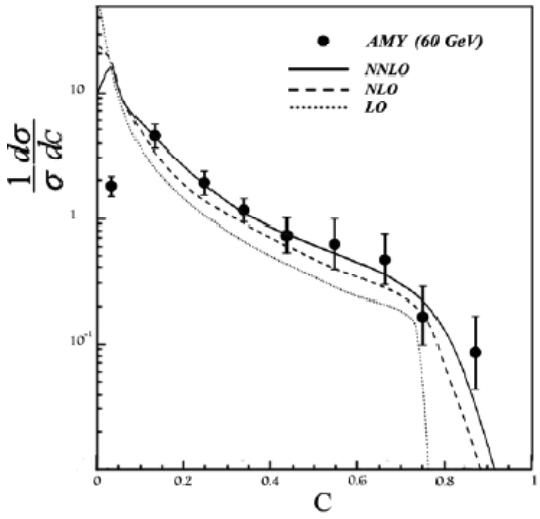

Fig. 12. The residual dependence of the fitted value of α_s and uncertainty $\chi 2$ on the renormalization scale.

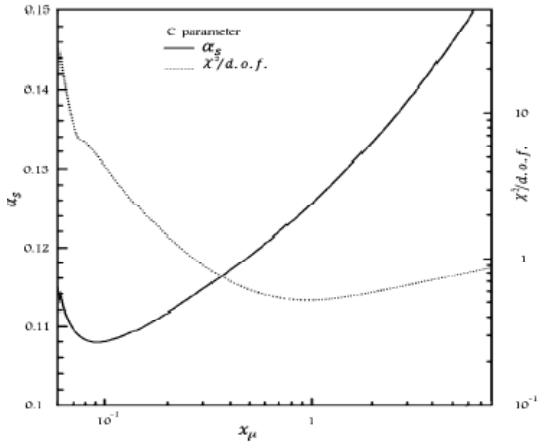

tions of clusters and remaining particles, until all the Y_{ij} values exceed Y_{cut}. The clusters remaining at this stage are defined as the jets.

The distribution of jet multiplicities obtained by these clustering algorithms depends on the jet defining parameter Y_{cut}. For small Y_{cut}, many jets are found because of the hadronization of the fluctuation process, whereas for large Y_{cut}, mostly two jet events are found and the $q\bar{q}g$ events are not resolved. However, Monte Carlo studies show that there is a range of cluster parameters for which QCD effects can be resolved and the fragmentation effects are sufficiently small. In the following, the parameter Y_{cut} = 0.04 is used, which is found to be a reasonable cut [11].

In Fig. 3, we show two- and three-jet fractions for different Y_{cut}. The decrease of the three-jet rate at large Y_{cut} is clearly visible. Our results are completely consistent with the results obtained by the JADE scheme [11, 12].

6. Altarelli–Parisi–Weizsacker–Williams technique

To calculate the α_s by this method, we work with the transverse momentum of the partons (Fig. 4) scaled to the e^+ (and e^-) beam energy,

$$X_T = \frac{2p_T}{Q} \tag{2}$$

Calculating the cross-section corresponding to the three-jet events, and using the Altarelli–Parisi–Weizsacker–Williams technique [21], we find

$$\frac{1}{\sigma}\frac{d\sigma}{dp_T^2} = \frac{4\alpha_s}{3\pi}\frac{1}{p_T^2}\mathrm{Log}\left(\frac{Q^2}{4p_T^2}\right) \tag{3}$$

where α_s is the quark–gluon coupling strength of QCD (first order). Fitting this expression, after integration, to the experimental P_T^2 distribution (Fig. 5), one obtains the value of α_s as 0.123 ± 0.004.

The value of α_s for different Y_{cut}s with respect to P_T^2 is listed in Table 1.

Using (2), the P_T^2 distribution (4) can be translated into distribution $d\sigma/dX_T^2$ [21]

$$\frac{1}{\sigma}\frac{d\sigma}{dX_T^2} = \frac{4\alpha_s}{3\pi}\frac{1}{X_T^2}\mathrm{Log}\left(\frac{1}{X_T^2}\right) \tag{4}$$

Fitting this expression, after integration, to the experimental X_T^2 distribution (Fig. 6), we obtain the value of α_s as 0.122 ± 0.004.

The value of α_s for different Y_{cut}s with respect to the X_T^2 is listed in Table 2.

7. Event shape variable

The properties of hadronic events may be described by a set of event shape observables. These may be used to characterize the distribution of particles in an event as "pencil-like", planar, spherical, etc. They can be computed either using the measured charged particles and calorimeter clusters or using the true hadrons or partons in simulated events. The following event shapes are considered here:

(*a*) *Thrust, T* [22]: The global event-shape variable thrust is defined as,

$$T = \max\left(\frac{\sum \boldsymbol{p}_i \cdot \boldsymbol{n}}{\sum |\boldsymbol{p}_i|}\right) \tag{5}$$

where $\boldsymbol{p}_i$ is the momentum vector of particle i, the thrust axis $\boldsymbol{n}$ is the unit vector that maximizes the above expression. The value of the thrust can vary between 0.5 and 1.0.

(*b*) *Heavy hemisphere mass,* M_H^2/s [23]: In the original definition, one divides the event into two hemispheres. In

Table 3. α_s values for different event shapes and their relative x_μ that uncertainty becomes minimized.

	T	ρ	B_T	B_W	C
α_s	0.124±0.004	0.125±0.006	0.122±0.003	0.124±0.005	0.114±0.008
x_μ	0.85	0.92	0.84	0.78	0.87

g. 13. Measurement of α_s from various experiments.

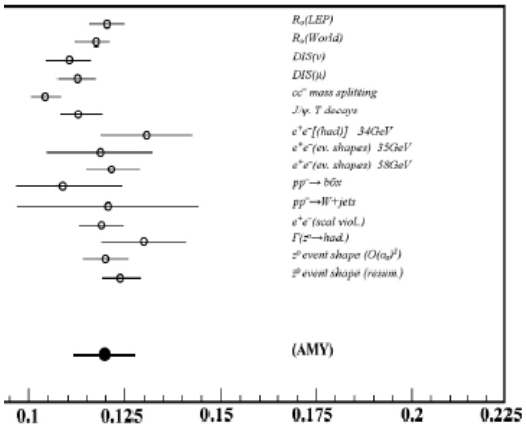

each hemisphere H_i one also computes the hemisphere invariant mass as,

$$\frac{M_i^2}{s} = \frac{1}{E_{\rm vis}^2}\left(\left(\sum_{k\in H_i} p_k\right)^2\right) \tag{6}$$

where $E_{\rm vis}$ is the total energy visible in the event. In the original definition, the hemisphere is chosen such that $M_1^2 + M_2^2$ is minimized. We follow the more customary definition whereby the hemispheres are separated by the plane orthogonal to the thrust axis. The larger of the two hemispheres invariant masses yields the heavy jet mass:

$$\rho \equiv \frac{M_H^2}{s} = \max\left(\frac{M_1^2}{s}, \frac{M_2^2}{s}\right) \tag{7}$$

) *Jet Broadening, B_W and B_T* [24]: Taking a plane perpendicular to n_T through the coordinate origin, one defines two events hemispheres $H_{1,2}$. In each, one determines the hemisphere broadening,

$$B_i = \frac{\sum_{k\in H_i} |p_k \times n_T|}{2\sum_k |pk|} \tag{8}$$

The wide and total jet broadening are then defined as,

$$B_W = \max(B_1, B_2) \tag{9}$$

$$B_T = B_1 + B_2 \tag{10}$$

') *The C parameter* [25]: The C-parameter is derived from the eigenvalues of the linearized momentum tensor,

$$\theta^{\alpha\beta} = \frac{1}{\sum_k |p_k|}\sum_k \frac{P_k^\alpha P_k^\beta}{|P_k|}, \qquad (\alpha, \beta = 1, 2, 3) \tag{11}$$

which has three eigenvalues λ_i. These eigenvalues are used to construct the C-parameter,

$$C = 3(\lambda_1\lambda_2 + \lambda_2\lambda_3 + \lambda_3\lambda_1) \tag{12}$$

This definition is equivalent to

$$C = 3(\theta^{11}\theta^{22} + \theta^{22}\theta^{33} + \theta^{33}\theta^{11} - \theta^{12}\theta^{12} - \theta^{23}\theta^{23} - \theta^{31}\theta^{31}) \tag{13}$$

8. Determination of α_s using event shape distributions

The perturbative expansion for the distribution of a generic observable y up to NNLO at e^+e^- centre-of-mass energy, $\sqrt{s}$, for a renormalization scale μ^2 is given by [26],

$$\begin{aligned}\frac{1}{\sigma_{\rm had}}\frac{{\rm d}\sigma}{{\rm d}y}(s,\mu^2,y) = &\left(\frac{\alpha_s(\mu)}{2\pi}\frac{{\rm d}\bar{A}}{{\rm d}y} + \left(\frac{\alpha_s(\mu)}{2\pi}\right)^2\right)\\ &\times\left(\frac{{\rm d}\bar{B}}{{\rm d}y} + \frac{{\rm d}\bar{A}}{{\rm d}y}\beta_0\log\frac{\mu^2}{s}\right)\\ &+\left(\frac{\alpha_s(\mu)}{2\pi}\right)^3\left(\frac{{\rm d}\bar{C}}{{\rm d}y} + 2\frac{{\rm d}\bar{B}}{{\rm d}y}\beta_0\log\frac{\mu^2}{s}\right.\\ &\left.+\frac{d\bar{A}}{dy}\left(\beta_0^2\log^2\frac{\mu^2}{s} + \beta_1\log\frac{\mu^2}{s}\right)\right) + O(\alpha_s^4)\end{aligned} \tag{14}$$

in which

$$\begin{aligned}\beta_0 &= \frac{11C_A - 4T_R N_F}{6}\\ \beta_1 &= \frac{17C_A^2 - 10C_A T_R N_F - 6C_F T_R N_F}{6}\end{aligned} \tag{15}$$

where the QCD colour factors are

$$C_A = N, \qquad C_F = \frac{N^2-1}{2N}, \qquad T_R = \frac{1}{2} \tag{16}$$

for $N = 3$ colours and N_F light quark flavours.

The coefficients $\bar{A}$, $\bar{B}$, and $\bar{C}$ have been computed for several event-shape variables [26, 27]. The calculation is carried out using a newly developed parton-level event generator programme EERAD3, which contains the relevant matrix elements with up to five external partons [28–31]. The measured normalized differential cross-sections for each of the 5 event shapes are shown in graphical form in Figs. 7–11. As the figures indicate, our real data are consistent with NNLO, compared with NLO or LO calculations, because it involves higher order terms in QCD calculations.

The value of α_s was estimated by fitting the data with (14). Separate fits were performed to each of the five observables at 60 GeV centre of mass energy.

In all these results, the uncertainty due to the choice of the renormalization scale $x_\mu = \mu/\sqrt{s}$ yields a large contribution to the total error. Consequently, missing higher orders, whose effects on the values of the coupling are assessed by varying x_μ, are still important. The fitted values for α_s change considerably for different choices of the scale. This is demonstrated for the *C*-parameter in Fig. 12. The plot shows the strong dependence of the fitted α_s on the renormalization scale factor x_μ. The real value of α_s was estimated by comparing theory with data using the minimum of $\chi 2$ in this figure, such that every where $\chi 2$ is minimum, its corresponding α_s becomes our real strong coupling constant. Averaging over different observables, indicated in Table 3, the mean value of α_s is determined to be 0.121 ± 0.007. This value is consistent with those obtained from different experiments [32–36].

Figure 13 shows the comparison of our measured value of α_s with that of other experiments [37].

9. Summary and conclusions

In this paper we present results obtained from a study of the structure of hadronic events at different centr-of-mass energies in electron–positron annihilations. We measure the momentum components with respect to the jet axis. The jet axis is defined by diagonalizing the momentum tensor for each event, namely the sphericity axis. Next we compare our results obtained by this method with various QCD models. At higher energies, the features of the gluon bremsstrahlung that leads to three-jet structures represent a gross violation of the parton model without gluons and find a most natural interpretation if gluon bremsstrahlung is included. Finally the coupling constant, α_s, is measured by two different methods, first by employing the jet clustering algorithm introduced by the JADE group. Using this method, the strong coupling constant is found to be 0.123 ± 0.004. Next, from the event shape distributions, we extract the strong coupling α_s, and test its evolution with energy scale. The results are consistent with the running of α_s, expected from QCD predictions. Averaging over different observables, the value of α_s is determined to be 0.121 ± 0.007.

References

1. P. Abreu et al. DELPHI Collaboration. Z. Phys. C, **70**, 179 (1996). doi:10.1007/s002880050095.
2. R. Barate et al. ALEPH Collaboration. Eur. Phys. J. C, **17**, 1 (2000). doi:10.1007/s100520000474.
3. M. Althoff et al. TASSO Collaboration. Z. Phys. C, **22**, 307 (1984).
4. G. Alexander et al. OPAL Collaboration. Z. Phys. C, **69**, 543 (1996). doi:10.1007/s002880050059.; K. Ackerstaff et al. OPAL Collaboration. Z. Phys. C, **75**, 193 (1997). doi:10.1007/s002880050462.
5. V.M. Abazov et al. DO Collaboration. Phys. Rev. D: Part. Fields, **65**, 052008 (2002). doi:10.1103/PhysRevD.65.052008.; S. Abachi et al. DO Collaboration. Phys. Rev. D : Part. Fields, **53**, 6000 (1996). doi:10.1103/PhysRevD.53.6000.
6. C. Adloff et al. H1 Collaboration. Eur. Phys. J. C, **5**, 625 (1998);; C. Adloff et al. H1 Collaboration. Eur. Phys. J. C, **6**, 575 (1999).
7. G. Sterman, J. Smith, J.C. Collins, J. Whitmore, R. Brock, J. Huston, J. Pumplin, W.-K. Tung, H. Weerts, C.-P. Yuan, S. Kuhlmann, S. Mishra, J.G. Morfín, F. Olness, J. Owens, J. Qiu, and D.E. Soper. Rev. Mod. Phys. **67**, 157 (1995). doi:10.1103/RevModPhys.67.157.
8. S.S. Adler, S. Afanasiev, C. Aidala, N.N. Ajitanand, Y. Akiba, J. Alexander, R. Amirikas, L. Aphecetche, S.H. Aronson et al. PHENIX Collaboration. Phys. Rev. Lett. **91**, 241803 (2003). doi:10.1103/PhysRevLett.91.241803. PMID: 14683109.
9. K. Maltman, D. Leinweber, P. Moran, and A. Sternbeck. PoS LATTICE2008, 214 arXiv:0812.2484 [hep-lat] (2008).
10. P.A. Baikov, K.G. Chetyrkin, and J.H. Kühn. Phys. Rev. Lett. **88**, 012001 (2001). doi:10.1103/PhysRevLett.88.012001. PMID:11800935.
11. G. Abbiendi et al. JADE and OPAL Collaboration. Eur. Phys. J. C, **17**, 19 (2000). doi:10.1007/s100520000432.
12. W. Bartel et al. JADE Collaboration. Z. Phys. C, **33**, 23 (1986). doi:10.1007/BF01410449.
13. V. Ravindran. Phys. Lett. **398B**, 169 (1997).
14. K.B. Lee et al. AMY Collaboration. Phys. Lett. **313B**, 469 (1993);; AMY Collaboration. Phys. Rev. D: Part. Fields, **41**, 2675 (1990). doi:10.1103/PhysRevD.41.2675.
15. O. Biebel. Phys. Rep. **340**, 165 (2001). doi:10.1016/S0370-1573(00)00072-7.
16. T. Kumita et al. AMY Collaboration. Phys. Rev. D: Part. Fields, **42**, 1339 (1990). doi:10.1103/PhysRevD.42.1339.
17. M. Althoff et al. TASSO Collaboration. Z. Phys. C, **22**, 307 (1984) . doi:10.1007/BF01547419.
18. C. Berger et al. PLUTO Collaboration. Z. Phys. C, **22**, 103 (1984). doi:10.1007/BF01572156.
19. D. Bender et al. HRS Collaboration. Phys. Rev. D: Part. Fields, **31**, 1 (1985). doi:10.1103/PhysRevD.31.1.
20. A. Petersen et al. MARK2 Collaboration. Phys. Rev. D: Part. Fields, **37**, 1 (1988). doi:10.1103/PhysRevD.37.1.
21. F. Halzen and A.D. Martin. Quarks and leptons. John Wiley, New York. 1984.
22. S. Brandt, C. Peyrou, R. Sosnowski, and A. Wroblewski. Phys. Lett. **12**, 57 (1964); E. Farhi. Phys. Rev. Lett. **39**, 1587 (1977). doi:10.1103/PhysRevLett.39.1587.
23. L. Clavelli and D. Wyler. Phys. Lett. **103B**, 383 (1981).
24. P.E.L. Rakow and B.R. Webber. Nucl. Phys. **B191**, 63 (1981). doi:10.1016/0550-3213(81)90286-8.; S. Catani, G. Turnock, and B.R. Webber. Phys. Lett. **295B**, 269 (1992).
25. G. Parisi. Phys. Lett. **74B**, 65 (1978); J.F. Donoghue, F.E. Low, and S.Y. Pi. Phys. Rev. D: Part. Fields, **20**, 3759 (1979).
26. A. Gehrmann-De Ridder, T. Gehrmann, E.W.N. Glover, and G. Heinrich. J. High Energy Phys. **12**, 094 [arXiv:0711.4711] (2007).
27. A. Gehrmann-De Ridder, T. Gehrmann, E.W.N. Glover, and G. Heinrich. Phys. Rev. Lett. **99**, 132002 [arXiv:0707.1285] (2007).
28. L.W. Garland, T. Gehrmann, E.W.N. Glover, A. Koukoutsakis, and E. Remiddi. Nucl. Phys. B, **627**, 107 (2002). doi:10.1016/S0550-3213(02)00057-3.; L.W. Garland, T. Gehrmann, E.W.N. Glover, A. Koukoutsakis, and E. Remiddi. Nucl. Phys. **B642**, 227 (2002). doi:10.1016/S0550-3213(02)00627-2.
29. S. Moch, P. Uwer, and S. Weinzierl. Phys. Rev. D: Part. Fields, **66**, 114001 hep-ph/0207043 (2002).
30. E.W.N. Glover and D.J. Miller. Phys. Lett. **396B**, 257 hep-

ph/9609474 (1997); Z. Bern, L.J. Dixon, D.A. Kosower, and S. Weinzierl. Nucl. Phys. **B489**. 3 (1997). doi:10.1016/S0550-3213(96)00703-1.; J.M. Campbell, E.W.N. Glover, and D.J. Miller. Phys. Lett. **409B**, 503 hep-ph/9706297 (1997); Z. Bern, L.J. Dixon, and D.A. Kosower. Nucl. Phys. **B513**, 3 (1998). doi:10.1016/S0550-3213(97)00703-7.

31. K. Hagiwara and D. Zeppenfeld. Nucl. Phys. **B313**, 560 (1989). doi:10.1016/0550-3213(89)90397-0.; F.A. Berends, W.T. Giele, and H. Kuijf. Nucl. Phys. **B321**, 39 (1989). doi:10.1016/0550-3213(89)90242-3.; N.K. Falck, D. Graudenz, and G. Kramer. Nucl. Phys. **B328**, 317 (1989). doi:10.1016/0550-3213(89)90331-3.
32. G. Alexander et al. OPAL Collaboration. Z. Phys. C, **72**, 191 (1996). doi:10.1007/s002880050237.
33. Y. Ohnishi et al. TOPAZ Collaboration. Phys. Lett. **313B**, 475 (1993).
34. D. Decamp et al. ALEPH Collaboration. Phys. Lett. **284B**, 163 (1992).
35. P. Abreu et al. DELPHI Collaboration. Z. Phys. C, **73**, 229 (1997). doi:10.1007/s002880050312.
36. M. Acciarri et al. L3 Collaboration. Phys. Lett. **411B**, 339 (1997).
37. Original references can be found in the reference of the plenary talk by S. Bethke at the 26th Int. Conf. on HENP, Dallas, Texas, USA. August 1992.